Front. Energy 2023, 17(4): 545–554
https://doi.org/10.1007/s11708-023-0867-7

RESEARCH ARTICLE

Juntian NIU, Cunxin ZHANG, Haiyu LIU, Yan JIN, Riguang ZHANG

Enhanced performance of oxygen vacancies on CO_2 adsorption and activation over different phases of ZrO_2

Abstract The effect of oxygen vacancies on the adsorption and activation of CO_2 on the surface of different phases of ZrO_2 is investigated by density functional theory (DFT) calculations. The calculations show that the oxygen vacancies contribute greatly to both the adsorption and activation of CO_2. The adsorption energy of CO_2 on the c-ZrO_2, t-ZrO_2 and, m-ZrO_2 surfaces is enhanced to 5, 4, and 3 folds with the help of oxygen vacancies, respectively. Moreover, the energy barrier of CO_2 dissociation on the defective surfaces of c-ZrO_2, t-ZrO_2, and m-ZrO_2 is reduced to 1/2, 1/4, and 1/5 of the perfect surface with the assistance of oxygen vacancies. Furthermore, the activation of CO_2 on the ZrO_2 surface where oxygen vacancies are present, and changes from an endothermic reaction to an exothermic reaction. This finding demonstrates that the presence of oxygen vacancies promotes the activation of CO_2 both kinetically and thermodynamically. These results could provide guidance for the high-efficient utilization of CO_2 at an atomic scale.

Keywords CO_2 activation, oxygen vacancies, ZrO_2, different phases

1 Introduction

The use of fossil energy has contributed to the development of modern industry. However, the greenhouse gas emission has caused a series of environmental and survival problems, such as global warming, sea level rise, land desertification, and reduction of grain [1–3]. The Paris Agreement, adopted at the 2015 UN Climate Summit, demonstrates the determination of the UN to curb the global warming trend. It is worth noting that CO_2 is a major greenhouse gas. The search for effective ways to collect and utilize CO_2 has become a hot research topic in recent years [4–6]. Currently, the main pathways to achieve chemical conversion of CO_2 include catalytic conversion of CO_2 to carbonate with alcoholic organics such as methanol or ethanol [7], reaction of CO_2 with hydrogen at a high temperature to produce methanol [8–14], and catalytic reforming of CO_2 with alkanes to prepare carbon monoxide and hydrogen [15]. CH_4 is also a type of greenhouse gas, whose greenhouse effect is 21 times more efficient than CO_2 [16].

The CO_2-CH_4 reforming process uses these two major greenhouse gases as feedstock. The syngas produced from reforming process is composed mainly of CO and H_2, which can be further synthesized by Fischer–Tropsch to produce high value-added chemicals or fuels [17–21]. Therefore, CO_2-CH_4 reforming into syngas has good prospects for application. The current technical means of CO_2-CH_4 reforming include steam reforming and dry reforming. Steam reforming was industrialized earlier [22,23], but the involvement of water in the reaction process had high requirements for the selection of the plant location. In contrast, the CO_2-CH_4 dry reforming (DRM) process is much more promising as it does not require the involvement of water. Actually, due to the high energy of C–H bond in CH_4 molecule ((107 ± 4) kcal/mol) [24], CH_4 molecule is uneasy to undergo activation reaction. Therefore, the choice of catalyst is extremely important for DRM reaction.

The catalyst for the DRM reaction mainly consists of two parts: the active metal and the support. When the active metal is a precious metal, the catalyst can obtain an excellent anti-carbon accumulation and thermal stability. However, the high cost makes it difficult to achieve a

Received Oct. 16, 2022; accepted Jan. 11, 2023; online Feb. 28, 2023

Juntian NIU (✉), Cunxin ZHANG, Haiyu LIU, Yan JIN
College of Electrical and Power Engineering, Taiyuan University of Technology, Taiyuan 030024, China
E-mail: juntianniu@163.com

Riguang ZHANG
State Key Laboratory of Clean and Efficient Coal Utilization, Taiyuan University of Technology, Taiyuan 030024, China

large-scale industrial application. Nickel has the highest activity among non-precious metals, but it is easily deactivated by sintering and carbon accumulation. The current research hotspot is to find a technical means to improve the comprehensive performance of nickel-based catalysts [25–29]. Many studies have pointed out that doping Ni with other transition metals, such as Cu, Fe, and Co, can improve its overall performance [30,31]. Meanwhile, finding a suitable support can also enhance the comprehensive performance of the catalyst. In fact, the support sometimes interacts synergistically with the active metal or even participates directly in the reaction itself [32–35]. This synergistic effect can greatly improve the comprehensive performance of the catalyst.

The supports of catalysts are generally prepared from metal oxides, and the commonly used supports are MgO, Al_2O_3, SiO_2, and ZrO_2. Among them, ZrO_2 has received a lot of attentions due to the presence of both acid-base centers and oxygen vacancies [36,37]. In 1993, Murota et al. [38] first reported that ZrO_2 could promote the ability of CeO_2 to store oxygen and lower the temperature at which the reduction reaction occurs from 1100 to 900 K. In 2014, Chen et al. [39] discovered that the higher the concentration of oxygen vacancies on the surface of ZrO_2 in the water–gas shift (WGS) reaction, the higher the catalytic efficiency of the catalyst. In 2017, Han et al. [40] found that the presence of oxygen vacancies on the ZrO_2 surface improved the selectivity of CH_4 during the hydrogenation of CO to CH_4. In 2021, Petchmark et al. [41] demonstrated that the ability of ZrO_2 to store hydrogen was increased in the presence of oxygen vacancies on its surface. These reports demonstrate that oxygen vacancies on the surface of ZrO_2 can improve its catalytic ability in various reactions. In fact, when ZrO_2 acts as a support, the oxygen vacancies can increase the contact area between the Ni particle and the support surface to keep the Ni particles well dispersed [42]. The high dispersion, on the other hand, allows the Ni particles to remain in a small size, and the particle size can directly affect the performance of the catalyst [43,44]. Overall, ZrO_2 reduces the carbon build-up of the catalysts at high temperatures and increases the activity when it is used as a support.

Currently, studies on the activation of the CH_4-CO_2 reforming process on the Ni/ZrO_2 catalyst surface using DFT and experimental methods have been reported [45–48]. However, studies on the effect of oxygen vacancies on the ZrO_2 surface on CO_2 adsorption and activation processes are still lacking. Elucidating the role of oxygen vacancies in CO_2 adsorption and activation is important for the preparation of high-performance DRM reaction catalysts using ZrO_2. Meanwhile, the metal oxides used as support generally exist in different crystalline phases, which can affect the performance of the catalyst [49,50]. Therefore, clarifying the differences in the adsorption and activation capacity of CO_2 on different phases of ZrO_2 surface is equally important.

In this paper, first, the energy barrier and adsorption energy of CO_2 on the perfect surfaces of different phases of ZrO_2 are obtained by DFT calculation. Next, oxygen vacancy (VO) is constructed on the surface of the different phases of ZrO_2. Afterwards, the adsorption energy and dissociation barrier of CO_2 on the defective ZrO_2 surface are calculated. Finally, the effect of the presence of oxygen vacancies on the ZrO_2 surface on CO_2 adsorption and activation is pointed out by comparison, and the results obtained throughout the study are summarized and their significance is discussed for the study of high-performance catalysts for CO_2 conversion.

2 Computational details

2.1 DFT method and parameter setting

In this paper, the Dmol3 module in Materials Studio 2019 (BIOVIA Ltd.) is used to complete the required density function theory (DFT) calculations [51,52]. The generalized gradient approximation (GGA) and the Perdue–Burke–Enzerhof (PBE) exchange-correlation general functions are used for exchange-correlation electron energies [53]. The valence electron wave function uses double numerical orbital basis set + d-orbit polarization (DND). The spin polarization of the electrons is considered in the calculation since ZrO_2 is a semiconductor. The vacuum layer is set to 20 Å to ensure that the intermolecular interaction forces between the plates are negligible. The calculated energy, force, and displacement convergence criteria are 2×10^{-5} Ha, 4×10^{-3} Ha/Å, and 5×10^{-3} Ha/Å, respectively. A smearing value of 0.05 Ha is used to ensure the accuracy of the calculation. Based on the Monkhorst–Pack method, the Brillouin zone integrals are selected with the sum approximation on the special k points. For the c-ZrO_2(111), t-ZrO_2(101), and m-ZrO_2(−111) surface models, the k values are taken as $2 \times 2 \times 1$, $3 \times 6 \times 2$, and $4 \times 3 \times 2$, respectively. The complete linear synchronous transfer and quadratic synchronous transfer (LST/QST) method was chosen to search for transition states and thus obtain the energy barrier of the reaction.

2.2 Model details

Thermodynamically stable surfaces of different phases of ZrO_2, i.e., c-ZrO_2(111) [54], t-ZrO_2(101) [55], and m-ZrO_2(−111) [56] are used in the study. The optimized perfect surface models of different phases of ZrO_2 are shown in Fig. S1 in Electronic Supplementary Material (ESM). For t-ZrO_2(101) and m-ZrO_2(−111), which have a good periodicity, both take two layers of O−Zr−O. For m-ZrO_2(−111), three O−Zr−O layers are taken. All the bottom O−Zr−O layer is fixed, while the rest is relaxed in

optimizing the surface model. The cell parameters used in the calculations fit well with those experimentally determined in previous reports, and the specific numerical comparisons are listed in Table 1.

2.3 Formula

In this paper, the adsorption energy E_{ads}, energy barrier E_b, and heat of reaction H of the reaction process are calculated by using Eqs. (1)–(3)

$$E_{ads} = E_{adsorbate/surf} - E_{adsorbate} - E_{surf}, \quad (1)$$

$$E_b = E_{TS} - E_{IS}, \quad (2)$$

$$H = E_{FS} - E_{IS}, \quad (3)$$

where $E_{adsorbate/surf}$ is the total energy of the metal surface with adsorbate on the surface, $E_{adsorbate}$ is the energy of the adsorbate alone, E_{surf} is the energy of the clear metal surface, E_{TS} is the energy of the transition state, E_{IS} is the energy of the reactants, and E_{FS} is the energy of the products.

3 Results and discussion

3.1 Construction of oxygen vacancies

The surface model with oxygen vacancy (V_O) is constructed as demonstrated in Fig. S2, with the oxygen vacancy sites being labeled. There are only 3-coordinated oxygen atoms on the surfaces of c-ZrO_2(111) and t-ZrO_2(101). Therefore, only one type of oxygen vacancy site is constructed, respectively. The defective c-ZrO_2(111) and t-ZrO_2(101) surfaces are denoted as c-ZrO_2^d(111) and t-ZrO_2^d(101), respectively. Three types of coordinated oxygen atoms are observed on the m-ZrO_2(−111) surface: 2-ligand, 3-ligand, and 4-ligand. Only the three oxygen atoms in the outermost layer are selected to construct the oxygen vacancy. The three oxygen vacancy sites are noted as V_{O1}, V_{O2}, and V_{O3} according to the horizontal depth of the oxygen vacancy on the model surface. Similarly, the latter is noted as m-ZrO_2^{d1}(−111), m-ZrO_2^{d2}(−111), and m-ZrO_2^{d3}(−111) in order for the m-ZrO_2(−111) surface with defects, where the coordination number of oxygen vacancies on the surfaces of m-ZrO_2^{d1}(−111) and m-ZrO_2^{d2}(−111) is 2, and the coordination number of oxygen vacancies on the surface of m-ZrO_2^{d3}(−111) is 3.

In addition, to clarify the ability of oxygen vacancies to accommodate the C and O atoms in CO_2, the adsorption energies of oxygen vacancies on the C and O atoms are calculated separately. The calculation results obtained are tabulated in Table 2.

The calculations show that the difference between the adsorption energy of the O atom and that of the C atom on the c-ZrO_2^d surface is the smallest, but still as high as 0.4 eV. On other defective surfaces, the adsorption energy of the O atom is about 1 eV higher than that of the C atom. It can, therefore, be assumed that in the presence of both C and O atoms, the oxygen vacancies on the ZrO_2 surface tend to adsorb O atoms. This is in line with previous reports [59]. However, it is worth noting that the adsorption energy of the C atom at the oxygen vacancy is above −2 eV, which is at a high level. Therefore, in the absence of free O atoms on the surface, the oxygen vacancies on the ZrO_2 surface may adsorb a certain amount of C atoms.

3.2 Adsorption of CO_2

The calculated most stable adsorption configurations of CO_2 on perfect and defective surfaces are exhibited in

Table 1 Lattice parameters of c-ZrO_2, t-ZrO_2, and m-ZrO_2 from X-ray crystallographic and their DFT optimized structures

Crystals and surface	Space group	DFT[a] (In this study)				X-ray[b] (Experimental measurement)			
		a	*b*	*c*	*β*	*a*	*b*	*c*	*β*
c-ZrO_2 (111)	Fm3m	5.14	5.14	5.14		5.09	5.09	5.09	
t-ZrO_2 (101)	P42/nmc	3.64	3.64	5.31		3.64	3.64	5.27	
m-ZrO_2 (−111)	P21/c	5.23	5.27	5.42	100.05	5.17	5.23	5.34	99.2

Notes: [a]——The *a*, *b*, and *c* parameters are in Å, and *β* is in degree; [b]——The parameters of c-ZrO_2, t-ZrO_2, and m-ZrO_2 were taken from Refs. [54,57,58], respectively.

Table 2 Comparison of adsorption energy of C atoms and O atoms on defective surfaces

Phase	Defective sites	Adsorption energy /eV	
		C	O
c	–	−3.38	−3.81
t	–	−2.29	−3.82
m	V_{O1}	−2.33	−3.31
	V_{O2}	−2.68	−3.61
	V_{O3}	−2.45	−3.43

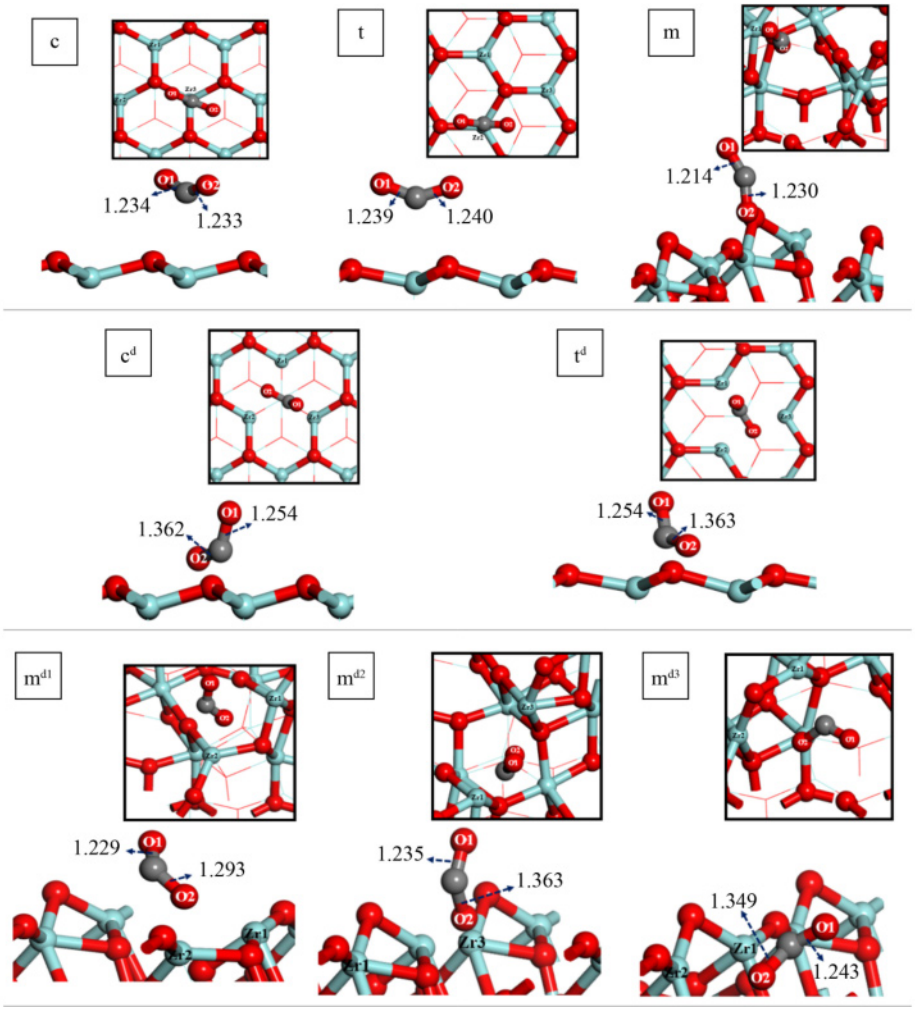

Fig. 1 Adsorption configurations of CO_2 on perfect and defective surfaces.

Fig. 1, and the adsorption energies are recorded in Table 3.

As the shown in Fig. 2(a), the adsorption energy of CO_2 on the defective surface is always greater than its adsorption energy on the perfect surface. The adsorption energy can be reduced by a maximum of 5-fold, as shown in Fig. 2(b). This indicates that the presence of oxygen vacancies can greatly facilitate the adsorption of CO_2 on the ZrO_2 surface. The largest increase in adsorption energy is found on the c-ZrO_2(111) surface, where the adsorption energy of CO_2 on the perfect surface is −0.198 eV, while on the defective surface the adsorption energy increases to −0.996 eV. For the m-ZrO_2(−111) surface, where V_{O3} is present, the increase in adsorption energy is minimal, but the adsorption energy of the defective surface can still be about 2.4 times higher than that of the perfect surface. Moreover, for t-ZrO_2(101), the involvement of oxygen vacancies increases the adsorption energy of CO_2 from −0.198 to −0.996 eV. In fact, for the m-ZrO_2(−111) surface, it is observed that the contribution of oxygen vacancies to the adsorption diminishes as they penetrate deeper into the surface.

Table 3 Adsorption energy of CO_2 adsorbed on perfect and defective surfaces of ZrO_2, respectively

Phase	Defective sites	Adsorption energy/eV	
		Defective surface	Perfect surface
c	–	−0.996	−0.198
t	–	−1.028	−0.226
m	V_{O1}	−0.999	−0.306
	V_{O2}	−1.003	
	V_{O3}	−0.728	

3.3 Activation of CO_2

The transition state models for the activation process of CO_2 on perfect and defective surfaces are obtained, as manifested in Fig. 3. The calculated energy barrier, reaction heat, and Mulliken atomic charge are presented in Table 4. The electron density of CO_2 binding on the surface of different phases of ZrO_2 are displayed in Fig. 4.

As shown in Fig. 5(a), the presence of oxygen

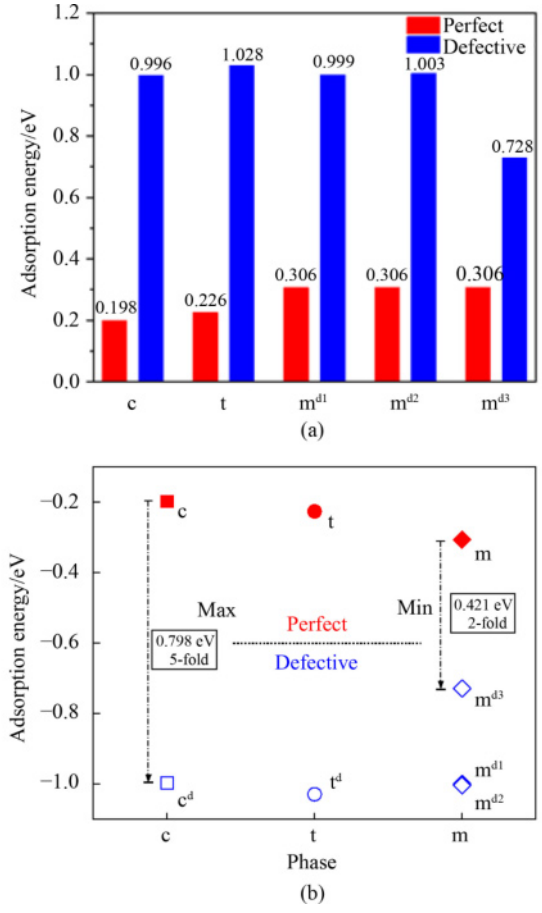

Fig. 2 CO_2 adsorption energy.

(a) Comparison of absolute values of CO_2 adsorption energy; (b) changes in CO_2 adsorption energy (red for perfect surfaces and blue for defective surfaces).

vacancies significantly reduces the energy barrier of CO_2 dissociation. The energy barrier of CO_2 dissociation can be reduced to a maximum of 1/5 of a perfect surface, as shown in Fig. 5(b). For m-ZrO_2^{d2}(−111), oxygen vacancies can reduce the energy barrier of CO_2 dissociation from 1.593 to 0.312 eV. For c-ZrO_2^{d}(111), the oxygen vacancy reduces the energy barrier from 1.671 to 0.463 eV, a reduction of roughly 3.6-fold. For t-ZrO_2^{d}(101), the energy barrier is reduced from 1.713 to 0.352 eV with the help of oxygen vacancies, a reduction of 4.9 times.

In addition, it can be observed from Fig. 6 that of the perfect surfaces, the m-ZrO_2(−111) and t-ZrO_2(101) surfaces are the most suitable for CO_2 activation, whereas, of the defective surfaces, the t-ZrO_2^{d}(101) surface is the most favorable for CO_2 activation, followed by m-ZrO_2^{d2}(−111). At the same time, the activation of CO_2 is transformed from an endothermic to an exothermic reaction on all defective surfaces. This suggests that oxygen vacancies can contribute kinetically and thermodynamically to the activation process of CO_2.

The nature of the oxygen vacancies that promotes CO_2 activation can be revealed clearly from the electron perspective. The Mulliken atomic charge listed in Table 4 indicates that oxygen vacancies could reduce the energy barrier of CO_2 dissociation by increasing the charge transfer from the ZrO_2 surface to the CO_2 molecule. For the c-ZrO_2^{d}(111) and t-ZrO_2^{d}(101) surface, the charge transfer can be increased about 2.8 times. For the m-ZrO_2^{d2}(−111) surface, the enhancement is up to 3.7 times. The electron density of the CO_2 molecule depicted in Fig. 4 then visually illustrates the intensity of the electron transfer between the CO_2 molecule and the ZrO_2

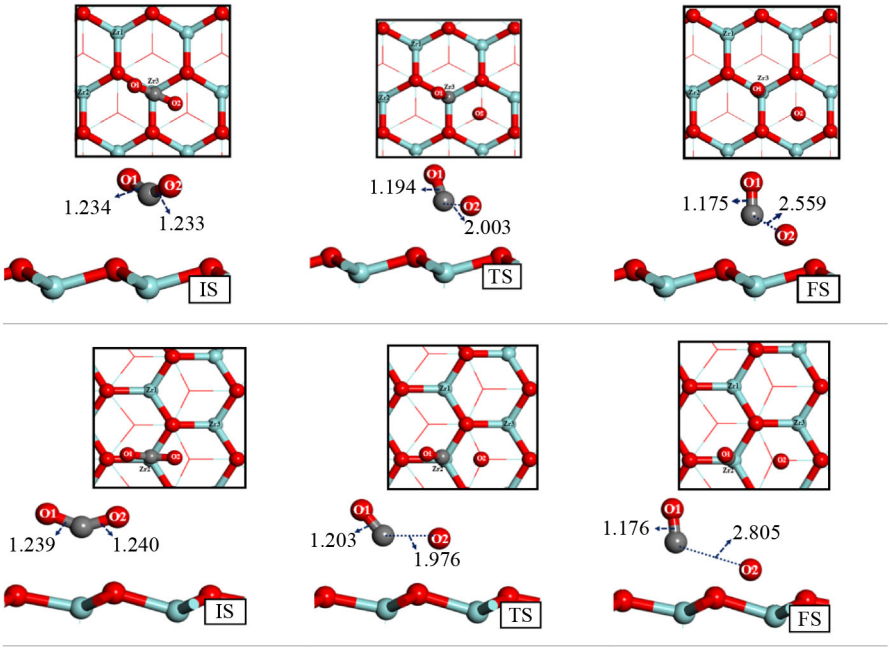

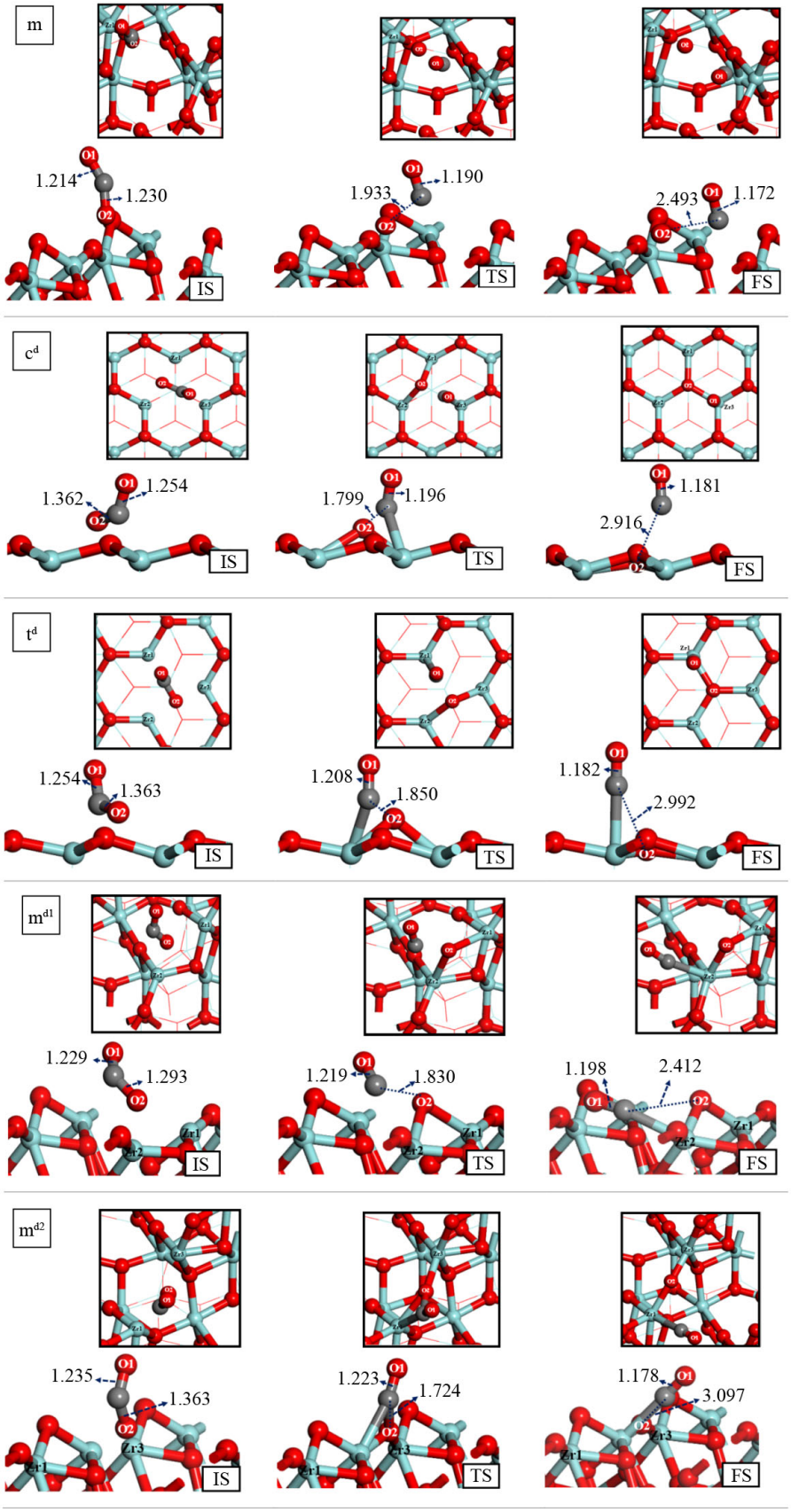
m
1.214
1.230
O1
O2
IS
1.933
1.190
TS
2.493
1.172
FS
c^d
1.362
1.254
1.799
1.196
2.916
1.181
t^d
1.254
1.363
1.208
1.850
1.182
2.992
m^d1
1.229
1.293
1.219
1.830
1.198
2.412
Zr1
Zr2
m^d2
1.235
1.363
Zr3
1.223
1.724
1.178
3.097

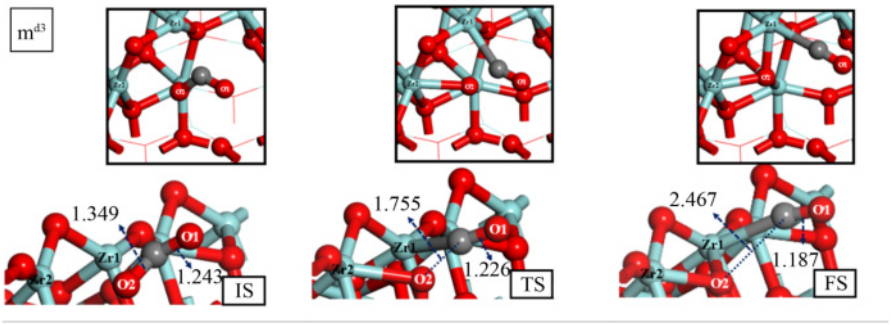

Fig. 3 Transition state model for activation process of CO_2 on perfect and defective surfaces (Oxygen atoms adsorbed on the surface are labeled O2 and O atoms retained in CO are labeled O1.).

Table 4 Energy barrier, reaction heat, and Mulliken atomic charge of CO_2 activation on perfect and defective surfaces

Phase	Defective sites	Energy barrier/eV		Reaction heat/eV		Mulliken charge/e	
		Perfect surface	Defective	Perfect surface	Defective surface	Perfect surface	Defective surface
c	–	1.671	0.463	1.511	−0.592	−0.230	−0.653
t	–	1.713	0.352	1.347	−0.663	−0.247	−0.667
m	V_{O1}	1.593	0.758	1.171	−0.306	−0.188	−0.464
	V_{O2}		0.312		−0.499		−0.701
	V_{O3}		0.436		−0.619		−0.585

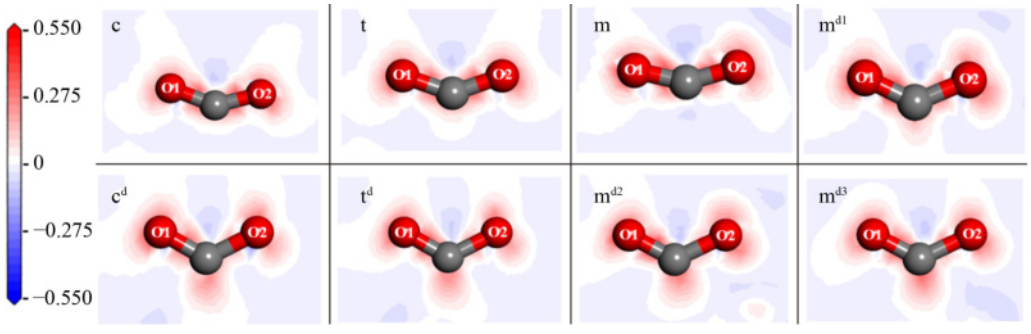

Fig. 4 Electron density of CO_2 binding on surface of different phases of ZrO_2.

surface. It can be noticed that oxygen vacancies greatly facilitate the charge exchange between the CO_2 molecule and the ZrO_2 surface.

4 Conclusions

The processes of CO_2 adsorption and activation on perfect and defective ZrO_2 surfaces are calculated separately in this paper. By comparing the results of the calculations, the following main conclusions can be drawn.

1) The oxygen vacancies on the ZrO_2 surface are more inclined to accommodate O atoms. Meanwhile, when CO is adsorbed on the ZrO_2 surface, the Zr atoms prefer to adsorb the C atom in CO.

2) The adsorption energy of CO_2 is greatest on m-ZrO_2(−111) and t-ZrO_2(101) surfaces in perfect surfaces, and it is greatest on t-ZrO_2^d(101) and m-ZrO_2^{d2}(−111) surfaces among the defective surfaces. In fact, the presence of oxygen vacancies greatly enhances the adsorption efficiency of CO_2 on the ZrO_2 surface. For the m-ZrO_2^{d3}(−111) surface, the oxygen vacancies increase the adsorption energy of CO_2 by a factor of more than two, and for c-ZrO_2^d(111) surfaces, the adsorption energy increases by a factor of fully five.

3) The energy barrier for CO_2 dissociation are lowest on t-ZrO_2(101) and m-ZrO_2(−111) surfaces in perfect surfaces while they are lowest on t-ZrO_2^d(101) and m-ZrO_2^{d2}(−111) surfaces in defective surfaces. The activation process of CO_2 is greatly facilitated by oxygen vacancies, both thermodynamically and kinetically. From a kinetic point of view, the energy barrier of CO_2 dissociation can be reduced to at most 1/5 of its initial

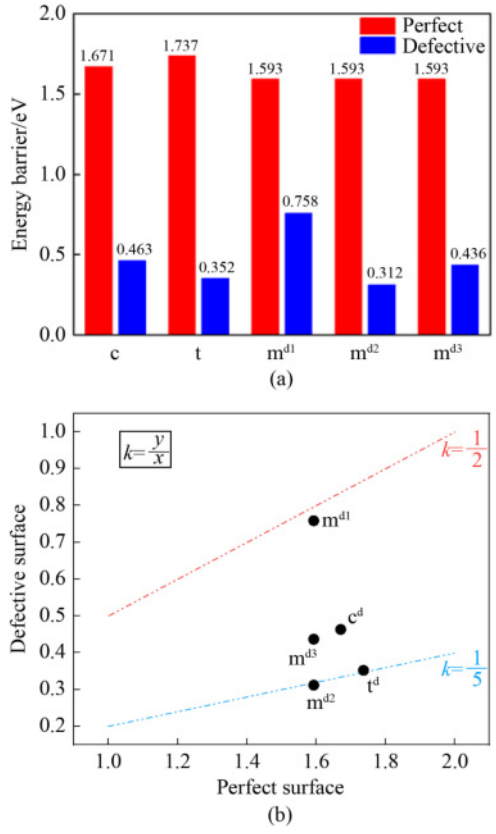

Fig. 5 CO_2 dissociation energy barrier.

(a) Comparison of absolute values of CO_2 dissociation energy barrier; (b) changes in energy barrier of CO_2 dissociation. (In Fig. (b), the horizontal and vertical coordinates represent the dissociation energy barrier of CO_2 on perfect and defective surfaces, respectively, and the k value is the ratio of the vertical to the horizontal coordinate.).

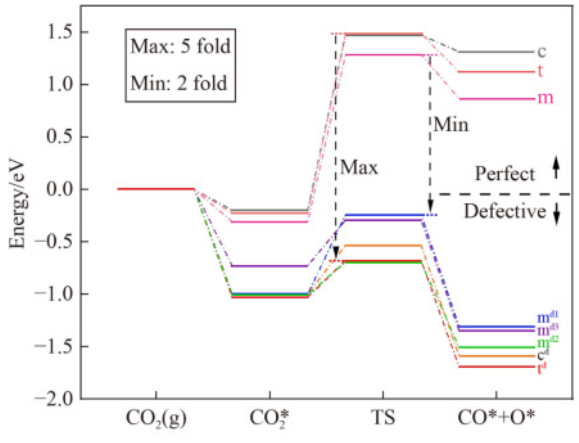

Fig. 6 Energy change curve (a value of Max means that the presence of oxygen vacancies can reduce the energy barrier to a maximum of 1/5 of the initial, and a value of Min means that the reduction is a factor of 1/2 similarly.).

value on the t-ZrO_2^d(101) and m-ZrO_2^{d2}(−111) surface. From the thermodynamic point of view, the activation process of CO_2 on the ZrO_2 surface of different phases changes from an absorbing to an exothermic reaction.

These results could indicate the outstanding contribution of oxygen vacancies to the adsorption and activation of CO_2, and provide guidance for the design of efficient DRM catalysts at an atomic scale.

Acknowledgements This work was supported by the National Natural Science Foundation of China (Grant No. 52106179) and the Fundamental Research Program of Shanxi Province, China (Grant No. 20210302124017).

Competing interests The authors declare that they have no competing interests.

Electronic Supplementary Material Supplementary material is available in the online version of this article at https://doi.org/10.1007/s11708-023-0867-7 and is accessible for authorized users.

References

1. Tollefson J. World looks ahead post-Copenhagen. Nature, 2009, 462(7276): 966–967
2. Tollefson J. Copenhagen: The scientists' view. Nature, 2009, 462(7274): 714–715
3. Wang W, Wang S, Ma X, et al. Recent advances in catalytic hydrogenation of carbon dioxide. Chemical Society Reviews, 2011, 40(7): 3703–3727
4. Valluri S, Claremboux V, Kawatra S. Opportunities and challenges in CO_2 utilization. Journal of Environmental Sciences (China), 2022, 113(3): 322–344
5. Wang X, Pan C, Romero C E, et al. Thermo-economic analysis of a direct supercritical CO_2 electric power generation system using geothermal heat. Frontiers in Energy, 2022, 16(2): 246–262
6. Wang H, He J. China's pre-2020 CO_2 emission reduction potential and its influence. Frontiers in Energy, 2019, 13(3): 571–578
7. Honda M, Tamura M, Nakagawa Y, et al. Ceria-catalyzed conversion of carbon dioxide into dimethyl carbonate with 2-cyanopyridine. ChemSusChem, 2013, 6(8): 1341–1344
8. Díez-Ramírez J, Díaz J A, Sánchez P, et al. Optimization of the Pd/Cu ratio in Pd-Cu-Zn/SiC catalysts for the CO_2 hydrogenation to methanol at atmospheric pressure. Journal of CO_2 Utilization, 2017, 22: 71–80
9. Frei M S, Mondelli C, Cesarini A, et al. Role of zirconia in indium oxide-catalyzed CO_2 hydrogenation to methanol. ACS Catalysis, 2020, 10(2): 1133–1145
10. Temvuttirojn C, Poo-arporn Y, Chanlek N, et al. Role of calcination temperatures of ZrO_2 support on methanol synthesis from CO_2 hydrogenation at high reaction temperatures over ZnO_x/ZrO_2 catalysts. Industrial & Engineering Chemistry Research, 2020, 59(13): 5525–5535
11. Numpilai T, Kidkhunthod P, Cheng C K, et al. CO_2 hydrogenation to methanol at high reaction temperatures over In_2O_3/ZrO_2 catalysts: Influence of calcination temperatures of ZrO_2 support. Catalysis Today, 2021, 375: 298–306
12. Witoon T, Chalorngtham J, Dumrongbunditkul P, et al. CO_2

hydrogenation to methanol over Cu/ZrO_2 catalysts: effects of zirconia phases. Chemical Engineering Journal, 2016, 293: 327–336
13. Witoon T, Numpilai T, Nijpanich S, et al. Enhanced CO_2 hydrogenation to higher alcohols over K-Co promoted In_2O_3 catalysts. Chemical Engineering Journal, 2022, 431: 133211
14. Witoon T, Lapkeatseree V, Numpilai T, et al. CO_2 hydrogenation to light olefins over mixed Fe-Co-K-Al oxides catalysts prepared via precipitation and reduction methods. Chemical Engineering Journal, 2022, 428: 131389
15. Stroud T, Smith T J, Le Saché E, et al. Chemical CO_2 recycling via dry and bi reforming of methane using $Ni\text{-}Sn/Al_2O_3$ and $Ni\text{-}Sn/CeO_2\text{-}Al_2O_3$ catalysts. Applied Catalysis B: Environmental, 2018, 224: 125–135
16. Rubin E S, Cooper R N, Frosch R A, et al. Realistic mitigation options for global warming. Science, 1992, 257(5067): 148–266
17. Anderson R B. Fischer-Tropsch Synthesis. New York: Academic Press, 1984
18. Schulz H. Short history and present trends of Fischer–Tropsch synthesis. Applied Catalysis A: General, 1999, 186(1−2): 3–12
19. Zhang C, Li Y, He Z, et al. Microtubular Fe/Mn-promoted $CaO\text{-}Ca_{12}Al_{14}O_{33}$ bi-functional material for H_2 production from sorption enhanced water gas shift. Applied Catalysis B: Environmental, 2022, 314: 121474
20. Van de Loosdrecht J, Botes F G, Ciobica I M, et al. Fischer-Tropsch synthesis: Catalysts and chemistry. In: Reedijk J, Poeppelmeier K, eds. Comprehensive Inorganic Chemistry II: From Elements to Applications. Elsevier, 2013: 525–557
21. Chen Y, Wei J, Duyar M S, et al. Carbon-based catalysts for Fischer–Tropsch synthesis. Chemical Society Reviews, 2021, 50(4): 2337–2366
22. Ashrafi M, Pröll T, Pfeifer C, et al. Experimental study of model biogas catalytic steam reforming: 1. Thermodynamic optimization. Energy & Fuels, 2008, 22(6): 4182–4189
23. Xu Y, Lausche A C, Wang S, et al. In silico search for novel methane steam reforming catalysts. New Journal of Physics, 2013, 15(12): 125021
24. Fattahi A, McCarthy R E, Ahmad M R, et al. Why does cyclopropene have the acidity of an acetylene but the bond energy of methane? Journal of the American Chemical Society, 2003, 125(38): 11746–11750
25. Lv J, Wang D, Wei B, et al. Integrated process of coal pyrolysis with dry reforming of low carbon alkane over $Ni/La_2O_3\text{-}ZrO_2$ with different La/Zr ratio. Fuel, 2021, 292: 120412
26. Fakeeha A H, Kurdi A, Al-Baqmaa Y A, et al. Performance study of methane dry reforming on Ni/ZrO_2 catalyst. Energies, 2022, 15(10): 3841
27. Lu Y, Guo D, Zhao Y, et al. Enhanced catalytic performance of Ni_x-V@HSS catalysts for the DRM reaction: The study of interfacial effects on Ni-VO_x structure with a unique yolk-shell structure. Journal of Catalysis, 2021, 396: 65–80
28. Qin Z, Chen L, Chen J, et al. Ni/CeO_2 prepared by improved polyol method for DRM with highly dispersed Ni. Greenhouse Gases. Science and Technology, 2021, 11(6): 1245–1264
29. Gao X, Lin Z, Li T, et al. Recent developments in dielectric barrier discharge plasma-assisted catalytic dry reforming of methane over Ni-based catalysts. Catalysts, 2021, 11(4): 455
30. Zhang L, Meng Y, Yang J, et al. Theoretical study on dry reforming of methane catalyzed by $Cu_{12}M$ (M= Cu, Fe, Co, Ni) core-shell bimetallic clusters. Fuel, 2021, 303: 121263
31. Qiu H, Ran J, Niu J, et al. Effect of different doping ratios of Cu on the carbon formation and the elimination on Ni(111) surface: A DFT study. Molecular Catalysis, 2021, 502: 111360
32. Ou Z, Ran J, Qiu H, et al. Uncovering the effect of surface basicity on the carbon deposition of Ni/CeO_2 catalyst modified by oxides in DRM. Fuel, 2023, 335: 126994
33. Hao S, Zhang H. High catalytic performance of nitrate reduction by synergistic effect of zero-valent iron (FeO) and bimetallic composite carrier catalyst. Journal of Cleaner Production, 2017, 167: 192–200
34. Yang W, Zhao H, Wang K, et al. Synergistic effects of mixtures of iron ores and copper ores as oxygen carriers in chemical-looping combustion. Proceedings of the Combustion Institute, 2015, 35(3): 2811–2818
35. Nagappagari L R, Samanta S, Sharma N, et al. Synergistic effect of a noble metal free $Ni(OH)_2$ co-catalyst and a ternary $ZnIn_2S_4/g\text{-}C_3N_4$ heterojunction for enhanced visible light photocatalytic hydrogen evolution. Sustainable Energy & Fuels, 2020, 4(2): 750–759
36. Chen H Y T, Tosoni S, Pacchioni G. A DFT study of the acid–base properties of anatase TiO_2 and tetragonal ZrO_2 by adsorption of CO and CO_2 probe molecules. Surface Science, 2016, 652: 163–171
37. Liang Z, Wang W, Zhang M, et al. Structural, mechanical and thermodynamic properties of ZrO_2 polymorphs by first-principles calculation. Physica B, Condensed Matter, 2017, 511: 10–19
38. Murota T, Hasegawa T, Aozasa S, et al. Production method of cerium oxide with high storage capacity of oxygen and its mechanism. Journal of Alloys and Compounds, 1993, 193(1−2): 298–299
39. Chen C, Ruan C, Zhan Y, et al. The significant role of oxygen vacancy in Cu/ZrO_2 catalyst for enhancing water–gas-shift performance. International Journal of Hydrogen Energy, 2014, 39(1): 317–324
40. Han X, Yang J, Han B, et al. Density functional theory study of the mechanism of CO methanation on $Ni_4/t\text{-}ZrO_2$ catalysts: Roles of surface oxygen vacancies and hydroxyl groups. International Journal of Hydrogen Energy, 2017, 42(1): 177–192
41. Petchmark M, Ruangpornvisuti V. Hydrogen adsorption on c-ZrO_2(111), t-ZrO_2(101), and m-ZrO_2(111) surfaces and their oxygen-vacancy defect for hydrogen sensing and storage: A first-principles investigation. Materials Letters, 2021, 301: 130243
42. Alioui O, Badawi M, Erto A, et al. Contribution of DFT to the optimization of Ni-based catalysts for dry reforming of methane: A review. Catalysis Reviews−Science and Engineering, 2022, online, https://doi.org/10.1080/01614940.2021.2020518
43. Zhu Z, Tao H, Zhou Y. Using density functional theory to unravel the size-dependent effect of Au nanoparticles and au single atoms adsorbed on carbon nitride for the hydrogenation of nitrobenzene. ACS Applied Nano Materials, 2022, 5(12): 18753–18760
44. Niu J, Chen S, Zheng X, et al. Understanding the effect of Ni cluster size on methane activation and dehydrogenation.

International Journal of Hydrogen Energy, 2022, online, https://doi.org/10.1016/j.ijhydene.2022.12.174

45. Fakeeha A H, Kurdi A, Al-Baqmaa Y A, et al. Performance study of methane dry reforming on Ni/ZrO_2 catalyst. Energies, 2022, 15(10): 3841
46. Hu X, Jia X, Zhang X, et al. Improvement in the activity of Ni/ZrO_2 by cold plasma decomposition for dry reforming of methane. Catalysis Communications, 2019, 128: 105720
47. Niu J, Liu H, Jin Y, et al. Comprehensive review of Cu-based CO_2 hydrogenation to CH_3OH: Insights from experimental work and theoretical analysis. International Journal of Hydrogen Energy, 2022, 47(15): 9183–9200
48. Niu J, Liu H, Jin Y, et al. A density functional theory study of methane activation on MgO supported Ni_9M_1 cluster: Role of M on C–H activation. Frontiers of Chemical Science and Engineering, 2022, 16(10): 1485–1492
49. Han L, Jing F, Zhang J, et al. Environment friendly and remarkably efficient photocatalytic hydrogen evolution based on metal organic framework derived hexagonal/cubic In_2O_3 phase-junction. Applied Catalysis B: Environmental, 2021, 282: 119602
50. Chen J, Abazari R, Adegoke K A, et al. Metal–organic frameworks and derived materials as photocatalysts for water splitting and carbon dioxide reduction. Coordination Chemistry Reviews, 2022, 469: 214664
51. Delley B. An all-electron numerical method for solving the local density functional for polyatomic molecules. Journal of Chemical Physics, 1990, 92(1): 508–517
52. Delley B. From molecules to solids with the $DMol_3$ approach. Journal of Chemical Physics, 2000, 113(18): 7756–7764
53. Perdew J P, Burke K, Ernzerhof M. Generalized gradient approximation made simple. Physical Review Letters, 1996, 77(18): 3865–3868
54. Gerald K. X-Ray diffraction powder pattern of metastable cubic ZrO_2. Journal of the American Ceramic Society, 1971, 54(10): 531–531
55. Toraya H, Yoshimura M, Somiya S. Calibration curve for quantitative analysis of the monoclinic-tetragonal ZrO_2 system by X-ray diffraction. Journal of the American Ceramic Society, 1984, 67(6): 119–121
56. Christensen A, Carter E A. First-principles study of the surfaces of zirconia. Physical Review B: Condensed Matter, 1998, 58(12): 8050–8064
57. Arce-Ramos J M, Grabow L C, Handy B E, et al. Nature of acid sites in silica-supported zirconium oxide: a combined experimental and periodic DFT study. Journal of Physical Chemistry C, 2015, 119(27): 15150–15159
58. Taoudi A, Laval J P, Frit B. Synthesis and crystal structure of three new rare earth oxyfluorides related to baddeleyite [LnOF; Ln= Tm, Yb, Lu]. Materials Research Bulletin, 1994, 29(11): 1137–1147
59. Steib M, Lou Y, Jentys A, et al. Enhanced activity in methane dry reforming by carbon dioxide induced metal-oxide interface restructuring of nickel/zirconia. ChemCatChem, 2017, 9(20): 3809–3813